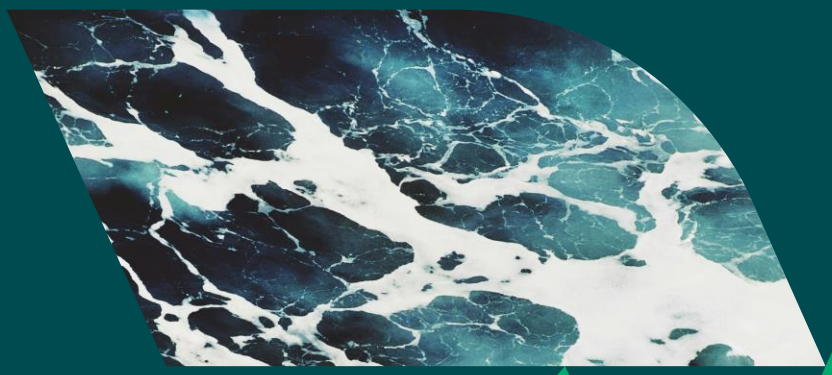

Insight into modelling offshore monopiles via 3D finite element analyses

venterra | GDG GAVIN & DOHERTY GEOSOLUTIONS

Proceedings of the XVIII ECSMGE 2024
GEOTECHNICAL ENGINEERING CHALLENGES
TO MEET CURRENT AND EMERGING NEEDS OF SOCIETY

ISBN 978-1-032-54816-6
DOI 10.1201/9781003431749-571

ECSMGE 24
XVIII EUROPEAN CONFERENCE
ON SOIL MECHANICS AND
GEOTECHNICAL ENGINEERING

Insight into modelling offshore monopiles via 3D finite element analyses

Considérations pour la modélisation de monopieux par élément finis 3D

D. Gaudio*
Dipartimento di Ingegneria Strutturale e Geotecnica, Sapienza Università di Roma, Rome, Italy

A.B. Batilas, L.M. Lapastoure, A. Loukas, J. Lee, T. Joseph, I. Thusyanthan
Gavin & Doherty Geosolutions, Dublin, UK

**domenico.gaudio@uniroma1.it*

ABSTRACT: Offshore wind farms have been attracting the attention of both researchers and practitioners over the past few decades, due to the growing interest in renewable energy. The choice of a particular foundation, which depends on several factors such as the mechanical properties of soil, depth to bedrock and bathymetry, may influence the overall wind farm cost by up to about 20%. Monopiles are the most used foundation system in the market, whose design can be further refined with advanced numerical analyses, provided that input parameters are properly calibrated. This paper shows the main results of a nonlinear static analysis of a monopile subjected to a horizontal load and embedded in a layered deposit. The analysis was performed using a 3D Finite Element model, where the foundation was represented with *plate* elements, and the soil mechanical behaviour was described with advanced constitutive models. The obtained pushover curves are shown and discussed, from which a reference design condition was selected. Then, the bending moment profile was obtained following three approaches, listed in a descending order of complexity: (1) integration of the stresses at the soil-*plate* interface; (2) derivation of the monopile rotation profile of the *plate* elements; (3) direct output from a *dummy beam* element located at the centreline of the monopile. It is shown that the *dummy beam* provides results in good agreement with those from the other two approaches, suggesting that it may be successfully adopted in practice to speed up the post-processing in the design of monopiles. The methodology presented in this paper would be useful for industrial projects.

RÉSUMÉ: Le développement des parcs éoliens en mer s'est accéléré au cours des dernières décennies grâce aux politiques publiques en matière d'environnement. Les monopieux sont le type de fondation le plus courant. Leur optimisation nécessite des modèles numériques avancés. Cet article présente les principaux résultats de la modélisation par éléments finis 3D d'un monopieu soumis à une charge horizontale. Dans cet exemple, le monopieux est installé dans un sol stratifié composé d'argile et de sable. Les résultats sont présentés en termes de déplacement et rotation du pieu sous l'effet du chargement latéral. L'évolution du moment de flexion le long du pieu est extrait de trois manières différentes: (1) par intégration des efforts à l'interface sol-pieu; (2) par dérivation du profil de rotation calculé à partir du déplacement des éléments coques qui modélisent le pieu; (3) à l'aide d'une poutre fictive modélisée au centre du pieu et qui permet de faciliter l'extraction des résultats. Cet exemple montre que les trois approches mènent à des résultats équivalents. Cela suggère que l'utilisation d'une poutre fictive peut être adoptée afin de faciliter et accélérer la modélisation des monopieux.

Keywords: Offshore wind turbines; monopiles; pushover analysis; 3D Finite Element model; *dummy beam.*

1 INTRODUCTION

Wind energy has emerged as a promising alternative energy source over the last few decades, to fill the world's energy supply and overcome some of the key issues associated with traditional fossil fuels, such as global warming. Particularly in Europe, offshore wind energy shows immense potential thanks to the presence of substantial portions of sea that are ideally suited for the construction of offshore wind farms (OWFs). Thanks to advancements in technology, OWFs have become profitable enough, despite their high construction costs, which depend not only on governmental subsidies, but also on private support. Most of the OWFs budget is allocated to foundation design, construction, and installation. Despite other solutions being under development, monopiles are still the most used type of substructure.

In this paper, the main preliminary results of a nonlinear static (*i.e.*, pushover) analysis of a monopile embedded in a layered deposit are presented. The analyses were carried out with the Finite Element (FE) code *Plaxis 3D* (Bentley, 2023a), considering advanced constitutive models, capable of capturing the nonlinear and irreversible behaviour of the soil. The

results of the analyses are first given in terms of force-displacement and force-rotation curves, together with the bending moment profile developed in the monopile. The latter was computed following three approaches, namely: (1) integration of the stresses at the soil-*plate* interface; (2) derivation of the rotation profile obtained from the *plate* elements representing the monopile; (3) extraction of direct output from a *dummy beam* element located at the centreline of the monopile. It is shown that the *dummy beam* provides results in good agreement with the other two strategies, which may suggest adopting it in the practice to speed up the post-processing step in the design of monopiles.

2 PROBLEM DEFINITION

Figure 1 shows the soil profile considered in the study, together with the geometry of the monopile. The soil profile is composed of two units, namely a clayey and a sandy layer. The layer thickness is equal to 5.2 m for the clay layer and 9.3 m for the sand layer. The water table is located 0.6 m below ground level.

The monopile is a hollow steel pile with an outer diameter $D = 2.0$ m, a wall thickness $t = 0.035$ m, a length $L = 11$ m ($L/D = 5.5$), and an embedment depth $H = 10.0$ m. Although the above dimensions are slightly smaller than those typically adopted for monopiles, they were considered in the numerical study for ease of numerical runs.

3 3D FINITE ELEMENT MODELLING

The Finite Element Analysis (FEA) was performed using the *Plaxis 3D* software to simulate the monotonic test under undrained conditions with a horizontal load applied atop the monopile, with a level arm $e = 0.5$ m with reference to the ground surface.

The mechanical clay behaviour was modelled using the *NGI-ADP* constitutive model (Grimstad *et al*., 2012), while the sand was simulated using the *HS-small* (*HSS*) model (Benz *et al*., 2009). The *NGI-ADP* constitutive model has been tailored to model the undrained behaviour of clays, matching both the undrained shear strength and strains at failure for three different stress paths *i.e.*, Active (s_u^A), Direct Simple Shear (s_u^{DSS}), and Passive (s_u^P). The *HSS* model is simple to calibrate and yet capable of capturing the key soil behaviour for the problem under consideration, such as a good representation of the stiffness at small strains and the non-linear stiffness behaviour with increasing strain.

The monopile was modelled using linear elastic, homogeneous and isotropic 6-node triangular *plate* elements with five degrees of freedom per node and quadratic shape functions, characterised by a wall thickness 0.035 m, a unit weight $\gamma = 78.5$ kN/m^3, a Young's modulus $E = 199.2$ GPa, and a Poisson's ratio $\nu = 0.3$. The modulus is slightly lower than that of steel, as a consequence of the code interpreting the input diameter as a centreline diameter: hence, the Young's modulus was corrected so that the bending stiffness *EI* remained unaffected.

The behaviour of the interface within the soil-monopile zone was modelled with linearly elastic-perfectly plastic *interface* elements, whose coefficient of reduction of the shear strength was equal to $R_{inter} = 0.7$ along the shaft and to $R_{inter} = 1.0$ at the base. The FE model consisted of 18117 elements, extending by 40 m along the *y*-axis and by 16 m along the *x*-axis (Figure 2), corresponding to $20 \cdot D$ and $16 \cdot D/2$, while the depth of the model was equal to 14.5 m. These model dimensions resulted from a preliminary sensitivity analysis, which showed that the boundaries did not affect the results when horizontal loads are applied atop the monopile. Also, they are in agreement with previous analyses performed on caisson foundations and onshore wind turbines under seismic loading (Gaudio *et al*., 2016; 2023).

In the analysis, the monopile was applied a horizontal force at the top, along the *y*-direction: therefore, half of the domain was only modelled, due to the symmetry of the problem.

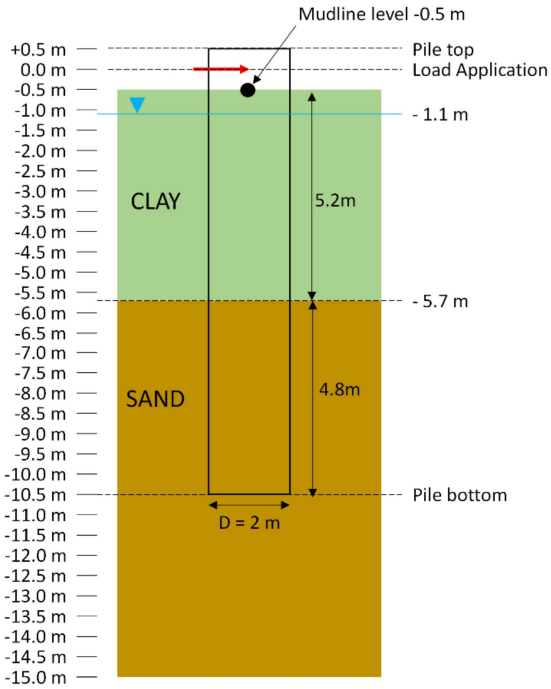

Figure 1. Soil profile and monopile geometry.

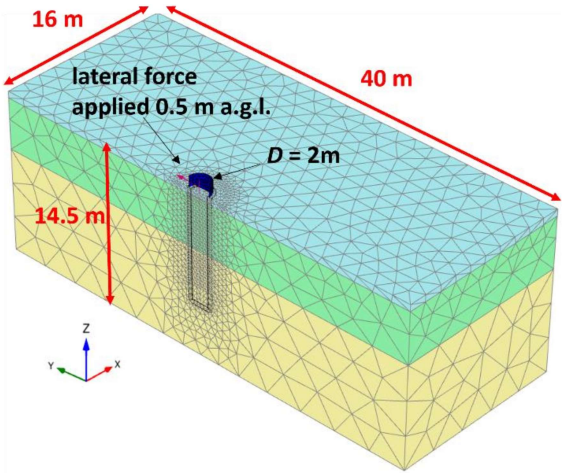

Figure 2. 3D Finite Element model adopted in the study.

3.1 Constitutive model soil parameters

The soil parameters of the constitutive models adopted in the FE analysis are listed in Table 1 and 2 for the *NGI-ADP* and the *HSS* models, respectively, which are representative of the mechanical behaviour of the clayey and sandy layers.

Table 1. NGI-ADP parameters for the clay layer.

Soil parameter	Value	Units
γ_{sat}	17	[kN/m^3]
γ'	7	[kN/m^3]
G_0/s_u^A	500	[-]
$s^A_{u,ref}$	60	[kPa]
$s^A_{u,inc}$	0	[kPa/m]
s_u^p/s_u^A	0.50	[-]
s_u^{DSS}/s_u^A	0.75	[-]
γ_f^C	12	[%]
γ_f^E	24	[%]
γ_f^{DSS}	18	[%]
τ_0/s_u^A	0	[-]
k_0	1	[-]

Table 2. HS-small parameters for sand layer.

Soil parameter	Value	Units
γ_{sat}	18	[kN/m^3]
γ'	8	[kN/m^3]
E_{50}^{ref}	69.6	[MPa]
E_{oed}^{ref}	69.6	[MPa]
E_{ur}^{ref}	208.7	[MPa]
G_0^{ref}	200	[MPa]
ν^{ur}	0.25	[-]
m	0.5	[-]
$\gamma_{0.7}$	0.015	[%]
φ'	40.0	[°]
φ'_{cv}	32.0	[°]
ψ	9.9	[°]
k_0	0.357	[-]
OCR	6	[-]

4 PUSHOVER CURVES

The results obtained from the nonlinear static analysis are discussed in this paragraph, which was performed as a *Plastic* calculation in Plaxis 3D. The monotonic response of the monopile is presented in Figure 3 in terms of the lateral load against the horizontal pile displacement and rotation of the monopile at the mudline level (see Figure 1).

As expected, the non-linear behaviour of the soil-monopile system was triggered from low levels of horizontal displacement. The displacement $y = D/10 = 0.20$ m is also marked in Figure 3, which was taken as a reference design condition for the assessment of the bending moment acting into the monopile, to compare against the yield moment, M_y, as discussed in the following section. The horizontal load $H_{0.1D} = 3076$ kN was computed for this design condition, which corresponded to a rotation $\theta = 1.49°$.

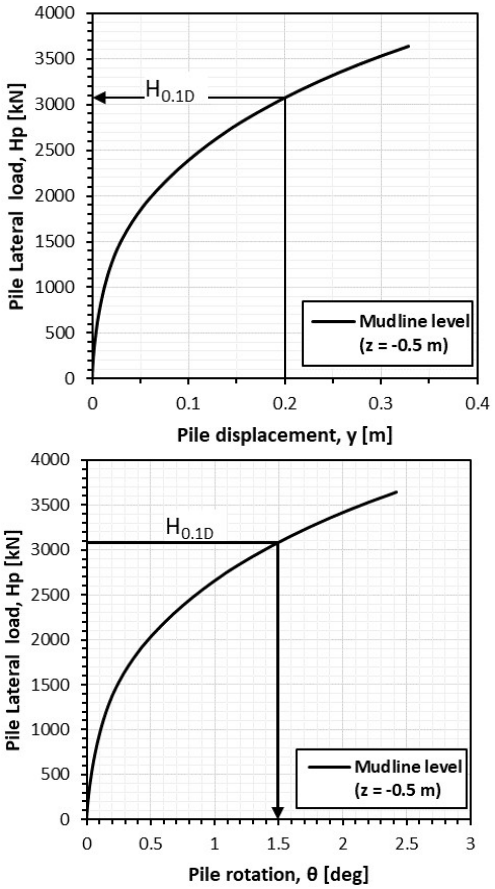

Figure 3. Monotonic pile response at the mudline level.

5 BENDING MOMENT PROFILES

The structural checks of the foundation were made by comparing the maximum bending moment

experienced by the monopile for the reference design condition mentioned above. To this end, the bending moment profile was first evaluated, following three different approaches, such as: (1) integration of the stresses at the soil-*plate* interface; (2) derivation of the rotation profile of the *plate* elements simulating the monopile; and (3) extraction of a direct output from the *dummy beam* element located at the centreline of the monopile.

The results obtained with the three approaches are compared in the next sections, after introducing them in a descending order of complexity.

5.1 Stress integration at the soil-*plate* interface

The bending moment profile was first calculated from the integration of stresses acting at the soil-*plate* interface as below:

$$M_{i,s} = H_p \times e + \int_0^{z_i} \left[p(z) \times \Delta z \right] \cdot dz + \int_0^{z_i} m(z) \cdot dz \quad (1)$$

where subscript i represents a depth counter (i = 1 m, 0.5 m, 0,…,-10.5 m), H_p is the lateral force applied atop the monopile, e = 0.5 m is the distance between the lateral load and the mudline level, $p(z)$ and $m(z)$ are the distributed lateral reaction and moment applied by the soil to the monopile, respectively, and Δz = 0.5 m is the depth interval selected for integration (Figure 4). The distributed lateral reaction $p(z)$ was computed from the integration of the interface forces along the y-direction, while the distributed moment, $m(z)$, was obtained from the integration of forces along the z-direction, multiplied by the respective lever arm $y = D/2$ = 1 m:

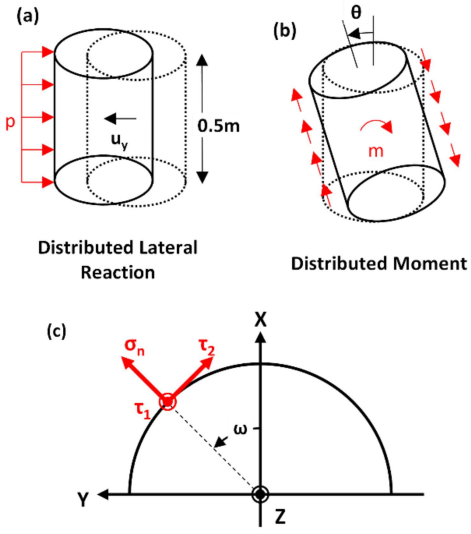

Figure 4. Distributed (a) lateral load p(z) and (b) moment m(z); (c) local coordinate system.

$$p(z) = \frac{\int_{z-\Delta z/2}^{z+\Delta z/2} F_y(z) \cdot dz}{\Delta z} \quad (2)$$

$$m(z) = \frac{\int_{z-\Delta z/2}^{z+\Delta z/2} F_z(z) \times y \cdot dz}{\Delta z} \quad (3)$$

where F_y and F_z are the forces along the y and z-direction, respectively.

Only stresses in local coordinates are accessible rather than forces F_y and F_z in the FE analysis, where σ_n is the stress normal to the interface, while τ_1 and τ_2 are the vertical and horizontal tangential stresses, respectively (Figure 4). The stresses were translated into forces as in eqs. (4) and (5) below, for every stress point, *i.e.*, for a given pair of coordinates, x and y, element area, A, and integration weight, w (Bentley, 2023b):

$$F_y(z) = w \cdot A \cdot \left[\sigma_n(z) \sin\omega - \tau_2(z) \cos\omega \right] \quad (4)$$

$$F_z(z) = w \cdot A \cdot \tau_1(z) \quad (5)$$

5.2 Derivative of rotations of *plate* elements

The bending moment profile was also calculated from the *plate* elements representing the monopile. To this end, the steps reported below were followed, starting from the vertical displacement of the two ends of the plates, whose sign convention is depicted in Figure 5:

- extraction of the back and front vertical displacement of the plate, $u_{z,i}^{front}$ and $u_{z,i}^{back}$, respectively;
- calculation of the pile rotation, θ_i, at the i^{th} depth (i = 1 m, 0.5 m, 0,…,-10.5 m) as:

$$\theta_i = \tan^{-1}\left(\frac{u_{z,i}^{back} - u_{z,i}^{front}}{D} \right) \quad (6)$$

- computation of the bending moment at the i^{th} depth (i = 1 m, 0.5 m, 0,…,-10.5 m), $M_{i,p}$, from the derivative of the pile rotation with depth (*i.e.*, curvature), where EI represents the bending stiffness of the monopile (E = Young's modulus, I = moment of inertia around the vertical axis) as:

$$M_{i,p} = EI \cdot \frac{d \tan\theta_i}{dz} = EI \cdot \left(\frac{\theta_i - \theta_{i+1}}{z_i - z_{i+1}} \right) \quad (7)$$

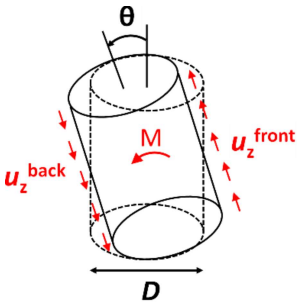

Figure 5. Calculation of the bending moment from plate elements.

5.3 Direct output from the *dummy beam*

Finally, the bending moment profile of the monopile was also obtained from a *dummy beam*, which was introduced at the centreline of the monopile. It is worth noting that this approach has already been routinely followed for excavation wall simulations in 2D conditions, when using continuum elements to model the wall and postprocessing the wall bending moments (Lam, 2018).

The stiffness of the *dummy beam* was selected to be low (*i.e.*, $E_{real}/E_{dummy} \approx 1000$) in order to not affect the results, as this beam was only used as a trick to avoid either integrating stresses acting along the shaft of the monopile or differentiating the *plate* rotation profile. Therefore, a Young's modulus $E_{dummy} = 210$ MPa was assigned to the *dummy beam* element, since the "real" Young's modulus of the monopile was the one of steel, $E_{real} = 199.2$ GPa (see § 3). As for the moment of inertia of the dummy beam, only half of the monopile inertia was considered thanks to the symmetry of the problem, *i.e.*, for the original diameter $D = 2$ m, the moment of inertia of the *dummy beam* was $I = 1/2 \cdot \pi/64 \cdot [D^4 - (D - 2t)^4] = 0.05216$ m^4. The bending moment profile was then extracted as follows:

$$M_{i,b} = \frac{(EI)_{real}}{(EI)_{dummy}} \times M_{dummy,i} = 1897 \times M_{dummy,i} \quad (8)$$

5.4 Comparison of bending moments profiles

A comparison of the bending moment profiles obtained with the three strategies above is made in Figure 6. The bending moments were computed for the design at the reference condition of a horizontal displacement $y = D/10 = 0.20$ m at mudline level. In the figure, the bending moment at yield, $M_y = 33.9$ MN·m, is also plotted.

From Figure 6 it is evident that the three solutions provide quite similar results, both in terms of the bending moment profile and its maximum value. In

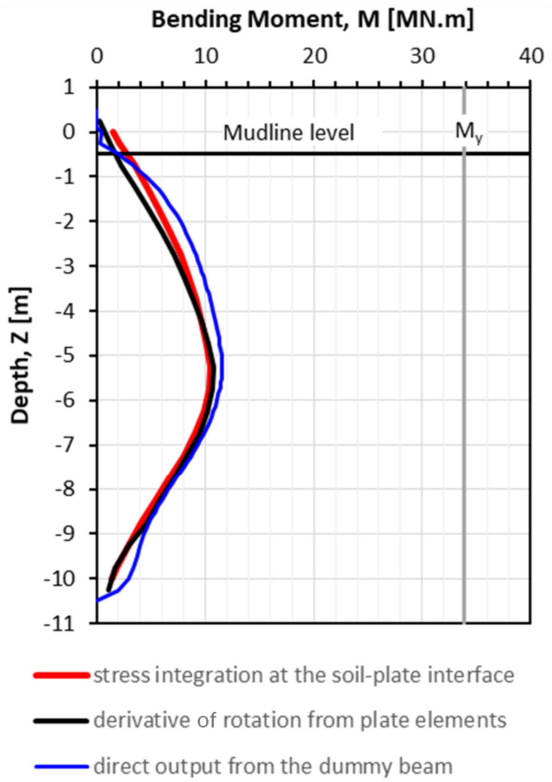

Figure 6. Bending moment profiles along the monopile computed with the three approaches adopted in the study.

particular, it is shown that the maximum bending moment from the stress integration (red line) was equal to $M_{max,\,s} = 10.4$ MN·m, while the one from the derivative of the monopile rotation (black) was equal to $M_{max,\,p} = 10.8$ MN·m, with negligible deviation of about 4.0%. As for the profile from the *dummy beam* (blue), the peak bending moment is equal to about $M_{max,\,b} = 11.5$ MN·m, which corresponded to an overestimation of 1.1 MN·m (~ 9.6%) and 0.7 MN·m (~ 6.1%) from the maximum values obtained from the stress integration and the derivative of rotations from the plate elements, respectively. This result shows that the *dummy beam* provides results in a good agreement with the other two strategies, which may suggest adopting it in the practice in the design of monopiles. Based on project experience of the Authors, the best method to derive the bending moment profile was the derivative of rotation from *plate* element method. The results above are summarised in Table 3.

Table 3. Summary of maximum bending moments (MN·m).

Approach	**Value [MN·m]**	***Comparison with the dummy beam***
stress integration	10.4	– 9.6%
rotation derivative	10.8	– 6.1%
dummy beam	11.5	/

6 CONCLUSIONS

The market of offshore wind turbines has been expanding over the last decades due to climate change, thereby increasing focus on the design of the foundation system, which can represent up to about 20% of the cost of the entire wind farm. Innovative solutions and design methods have therefore been sought to reduce costs of the foundation system.

In this paper, the results of a 3D Finite Element pushover analysis conducted on a monopile embedded in a layered deposit have been presented. In the analyses, the monopile was simulated through *plate* elements and subject to a horizontal force applied to the top of the foundation. The resulting force-displacement and force-rotation pushover curves have been first shown and discussed to detect a reference design condition for the monopile, corresponding to a horizontal displacement at the mudline level equal to one tenth of the outer diameter.

Then, the bending moment profile developed in the monopile has been computed. For the design condition, three different approaches have been used to determine this profile which include the integration of the stresses at the soil-*plate* interface, the derivation of the rotation profile obtained from the *plate* elements representing the monopile, and the extraction of direct output from a *dummy beam* located at the centreline of the monopile. It has been shown that the *dummy beam* provides results in good agreement with the other two strategies, which may suggest adopting it in the practice to speed up the post-processing step in the design of monopiles. It is worth noting that the Timoshenko's beam theory has been adopted in this study, which means that the beam deflection comes both from bending and shearing. This is expected to be well representative of the real behaviour for the monopile at hand. A discussion on the pitfalls of the deterministic approach followed for the *dummy beam* is given in Beck and Silva Jr. (2011).

The capability of 3D Finite Element models of capturing the main features of the soil-monopile behaviour under consideration would always involve a level of uncertainty. It is recommended that these models and results are validated using field-test results or case histories from existing literature.

ACKNOWLEDGEMENTS

The first author is grateful for the financial support provided by Ministero dell'Università e della Ricerca (Italy) through the project PON "Ricerca e Innovazione" 2014-2020.

REFERENCES

Beck, A. T., da Silva Jr, C. R. (2011). Timoshenko versus Euler beam theory: Pitfalls of a deterministic approach. *Structural Safety*, 33(1): 19-25, https://doi.org/10.1016/j.strusafe.2010.04.006.

Bentley (2023a). *PLAXIS 3D 2023.1: General Information Manual 3D* (Available at: https://communities.bentley.com/cfs-file/__key/communityserver-wikis-components-files/00-00-00-05-58/PLAXIS_5F00_3D_5F00_2023.1_5F00_3D_5F00_0_5F00_-General-Information-Manual.pdf, accessed: 12/03/2024).

Bentley (2023b). *PLAXIS 3D 2023.1: Scientific Manual 3D* (Available at: https://communities.bentley.com/cfs-file/__key/communityserver-wikis-components-files/00-00-00-05-58/PLAXIS_5F00_3D_5F00_2023.1_5F00_3D_5F00_4_5F00_-Scientific-Manual.pdf, accessed: 12/03/2024).

Benz, T., Vermeer, P. A., Schwab, R. (2009). A small-strain overlay model. *International Journal for Numerical and Analytical Methods in Geomechanics*, 33(1): 25-44, https://doi.org/10.1002/nag.701.

Gaudio, D., Rampello, S. (2016). Dynamic soil-structure interaction of bridge-pier caisson foundations. In *Geotechnical engineering in multidisciplinary research: from microscale to regional scale CNRIG2016. VI Italian Conf. of Researchers in Geotechnical Engineering, Procedia Engineering*, Elsevier, 158: 146-151, https://doi.org/10.1016/j.proeng.2016.08.420.

Gaudio D., Seong J., Haigh S., Viggiani G. M. B., Madabhushi G. S. P., Shrivatsava R., Veluvolu R., Padhy P. (2023). Boundary effects on dynamic centrifuge modelling of onshore wind turbines on liquefiable soils. *International Journal of Physical Modelling in Geotechnics*, ICE Publishing, 23(1): 16-34, ISSN: 1346-213X, https://doi.org/10.1680/jphmg.21.00085.

Grimstad, G., Andresen, L., Jostad, H. P. (2012). NGI-ADP: Anisotropic shear strength model for clay. *International Journal for Numerical and Analytical Methods in Geomechanics*, 36(4): 483-497, https://doi.org/10.1002/nag.1016.

Lam, A. K. (2018). An engineering solution for a hillside project in Hong Kong. *Geotechnical Research*, ICE Publishing, 5(3), 170-181, https://doi.org/10.1680/jgere.18.00008.


venterra